ELSEVIER

Journal of Fluids and Structures 23 (2007) 681–701

JOURNAL OF FLUIDS AND STRUCTURES

www.elsevier.com/locate/jfs

Forced streamwise oscillations of a circular cylinder: Locked-on modes and resulting fluid forces

Q.M. Al-Mdallal[a,1], K.P. Lawrence[b,*,1], S. Kocabiyik[c]

[a]*Department of Mathematical Sciences, United Arab Emirates University, Al-Ain, P.O. Box 17551, United Arab Emirates*
[b]*Department of Civil Engineering, University of Waterloo, Waterloo, Ont., N2L 3G1 Canada*
[c]*Department of Mathematics and Statistics, Memorial University of Newfoundland, St. John's, Nfld., A1C 5S7 Canada*

Received 9 August 2005; accepted 3 November 2006
Available online 23 April 2007

Abstract

A computational study of laminar, incompressible flow past a cylinder oscillating in the streamwise direction is performed using the two-dimensional unsteady Navier–Stokes equations in nonprimitive variables. The method of solution is based on a conjugating Fourier spectral analysis with finite-difference approximations. The numerical simulations are conducted at a fixed Reynolds number, $R = 200$, and at displacement amplitude-to-cylinder diameter of $A = 0.1$ and 0.3. Results show the existence of symmetric/asymmetric modes of vortex formation in the cylinder wake at different values of unsteady loading on the cylinder, which is characterized by the ratio of oscillation frequency, f, to Kármán vortex-shedding frequency, f_0. For this paper, the frequency ratio is chosen from $f/f_0 = 0.5$ to 3, where switching from asymmetric to symmetric vortex shedding is observed. The relation between these vortex-shedding modes and fluid forces on the cylinder surface is discussed. An analysis of the locked-on modes via Lissajous patterns of unsteady lift coefficient is also included. Previously computed and observed flow fields as well as fluid forces are compared to current numerical results and agreement is found to be excellent.

Keywords: Unsteady; Viscous; Incompressible; Vortex formation; Lock-on; Forced streamwise oscillation; Fluid forces

1. Introduction

The flow around oscillating bluff bodies is an important engineering problem both from the academic and practical points of view. Examples are chimney stacks, transmission lines, cables of suspended bridges, offshore structures and risers, which are exposed to wind or ocean currents. The practical significance of this type of flow has led to a large number of fundamental studies, many of which are discussed in the comprehensive reviews of King (1977), Sarpkaya (1979, 2004), Naudascher (1987), Griffin and Hall (1991), Bearman (1984), Matsumoto (1999), Pier and Huerre (2001), Williamson and Govardhan (2004); and in book chapters by Naudascher and Rockwell (1994), Zdravkovich (1997), Sumer and Fredsøe (1997) and Anagnostopoulos (2002).

*Corresponding author.
E-mail address: kp2lawre@uwaterloo.ca (K.P. Lawrence).
[1]Research conducted while first and second authors were at Memorial University of Newfoundland.

0889-9746/$ - see front matter © 2007 Elsevier Ltd. All rights reserved.
doi:10.1016/j.jfluidstructs.2006.11.001

In the present work, we are concerned with forced streamwise oscillations of a circular cylinder placed horizontally in a uniform stream of a viscous incompressible fluid. Initially, a cylinder of infinite extent is immersed, and remains fixed in a fluid flowing with free-stream velocity U, so that the longitudinal axis of the cylinder coincides with the z-axis of the Cartesian coordinate system. The flow is assumed to be unsteady, laminar and two-dimensional. At time $t^* = 0$ the cylinder impulsively starts to perform time-dependent sinusoidal oscillations in the streamwise (x) direction only with a displacement represented by $X^*(t^*) = -X^*_m \cos(2\pi f^* t^*)$. Here t^* is the dimensional time; X^*_m and f^* are the dimensional amplitude and forcing frequency of cylinder displacement, respectively. The characteristic length and velocity scales are taken to be the cylinder diameter d and free-stream velocity U, respectively. The dimensionless parameters are the Reynolds number, $R = Ud/\nu$, where ν is the kinematic viscosity of the fluid; the amplitude of the cylinder oscillation $A(= X^*_m/d)$; and the frequency ratio f/f_0, with $f = df^*/U$, and $f_0 = df^*_0/U$ being the dimensionless natural vortex-shedding frequency of a stationary cylinder. Thus the dimensionless cylinder displacement is $X(t) = -A\cos(2\pi ft)$, where $t = Ut^*/d$ is the dimensionless time.

The majority of previous studies have concentrated on the phenomenon of vortex-shedding lock-on (or synchronization) due to either forced or self-induced transverse oscillation of circular cylinders since the fluctuating lift is the dominant force. It was only in the early 1970s that King et al. (1973), King (1974) and Wootton et al. (1974) reported that streamwise vibrations can occur for full scale piles (or cantilevers) in an ocean current. For streamwise oscillations, the range near $f/f_0 \approx 2$ constitutes the fundamental lock-on regime. The developing downstream wake in conjunction with the entirely horizontal forcing of cylinder results in a lift coefficient with an irregular behavior as reported by Kim (2000) and Karanth et al. (1995). This irregularity of the lift coefficient poses difficulty in confirming the lock-on phenomenon through the classical power spectral density analysis. Taking this into account, in this study, the locked-on flow regimes are analyzed via Lissajous patterns of unsteady lift coefficient. Defining the reduced velocity as $V_r = U/f_n d$ with f_n being the natural frequency of a cylinder, the most important feature of a rigid spring-mounted circular cylinder free to oscillate in the streamwise direction is the existence of two excitation regions separated by the lock-on region found in the forced oscillation studies, which occurs around $V_r(= U/f_n d \leftrightarrow 1/f) \approx 1/2f_0 \approx 2.5$: symmetric vortex shedding for $V_r < 1/2f_0$ and alternating vortex streets for $V_r > 1/2f_0$. The ranges found in forced oscillation tests at low-oscillation amplitudes (Nishihara et al., 2005) agree well with the two streamwise excitation regions observed in free oscillation tests at large oscillation amplitude cases (King et al., 1973; King, 1974; Nakamura et al., 2001a, b; Okajima et al., 2002, 2004; Sakai et al., 2001). These experimental studies are conducted for high Reynolds number flows.

One approach to understanding these two instability regions has been to conduct experiments using forced streamwise oscillation of a cylinder in a uniform stream. Griffin and Ramberg (1976) demonstrated that at a Reynolds number of $R = 190$ the vortex shedding locks onto the forcing frequency over a range of frequencies from 120% to 250% of the natural shedding frequency (i.e., $f/f_0 \in [1.2, 2.5]$). They observed two different asymmetric modes of vortex formation in the wake at relatively low amplitudes ($0.06 \leqslant A \leqslant 0.22$) which correspond loosely to the known 2S and 2P modes observed in transverse cylinder oscillations where two single and two pairs of vortices, respectively, are shed per cycle (Williamson and Roshko, 1988). The asymmetric 2S mode corresponds to the classical Kármán vortex street type of mode found for cantilevers. Ongoren and Rockwell (1988) observed both cantilever modes of vortex formation at the small amplitude of $A = 0.13$ and at a dimensionless frequency, f, of 0.1–0.8 and investigated the mode competition in the near-wake. As f/f_0 is increased from 1.8 to 2.0, the mode of formation changed from the asymmetric 2S mode to asymmetric locked-on mode where one vortex pair and a single vortex were formed per cycle (P + S mode as originally defined by Williamson and Roshko). At $f/f_0 = 3.0, 4.0$, they observed additional lock-on states with the symmetric vortex pair mode described earlier for cantilever studies: symmetric two single counter-rotating vortices are shed in phase from both sides of the cylinder per cycle. The phenomenon of the formation of symmetric "twin" vortices was also reported by Barbi et al. (1986) when the cylinder is stationary and the incident mean flow has a low-amplitude periodic component superimposed upon it at a lower frequency ratio of $f/f_0 = 1$. For relatively low amplitudes (Konstantinidis et al., 2005), the wake pattern does not seem to change and remains at the 2S mode of Williamson and Roshko. In these experimental studies, no attempt was made to measure fluctuating fluid forces, and only qualitative information can be found except in the study by Konstantinidis et al. (2005) in which the forced wake was analyzed quantitatively in terms of the phase-referenced vorticity patterns and the timing of the vortex-shedding process.

Forced streamwise oscillation tests by Cetiner and Rockwell (2001) and Nishihara et al. (2005) focused on the precise measurements of fluid forces as well as detailed flow visualizations of wake patterns. Cetiner and Rockwell (2001) addressed the relationship between the fluid forces and the patterns of vorticity and streamline topology in the near-wake through the time-averaged spectra of the forces. Their investigation is performed over the range of Reynolds numbers $405 \leqslant R \leqslant 2842$, frequency ratio $0.37 \leqslant f/f_0 \leqslant 2.27$ and Keulegan–Carpenter number $1 \leqslant \mathrm{KC}(= 2\pi A) \leqslant 10$. Their study demonstrated that for sufficiently large KC and sufficiently low-normalized velocity $U/(2\pi fA)$, the lock-on

regimes are attainable for frequency ratios close to 0.5, 1.0 and 2.0. The maximum of dimensionless peak amplitude of the streamwise vortex-induced vibrations is less than 0.2. Taking this into account Tanida and Watanabe (1973) measured unsteady drag on a circular cylinder in a streamwise oscillation at $A = 0.14$ but sufficient data to discuss the excitation mechanism has not been obtained. Nishihara et al. (2005) investigated the relation between the unsteady drag force and the wake patterns at subcritical Reynolds numbers and $A = 0.05$ over the frequency ratio range $0.5 \leqslant f/f_0 \leqslant 4.0$ in order to verify the excitation mechanism of streamwise vortex-induced vibration.

The flow field behind a cylinder placed in a uniform stream and forcibly oscillated at a specified amplitude and frequency have also received attention from computationalists. Some of the above-mentioned phenomena of streamwise oscillations have been confirmed by two-dimensional numerical simulations. Hurlbut et al. (1982) considered three distinct forced oscillation cases: oscillations in a quiescent fluid; streamwise or transverse oscillations in a uniform stream. Their investigation is based on a finite-difference scheme to solve the Navier–Stokes equations in primitive variables. For the streamwise oscillation case, simulations are conducted at $R = 80, 100 : A = 0.14$ and $0 < f/f_0 \leqslant 2.5$. Using a compact finite-difference scheme, Lecointe and Piguet (1989) simulated flow past a circular cylinder that is simple harmonic and in the streamwise or transverse direction. For the streamwise oscillation case, simulations are conducted at $R = 200,\ 855 : 0.13 \leqslant A \leqslant 0.5$ and $0.8 \leqslant f/f_0 \leqslant 3.0$. Mittal et al. (1991) used a stabilized space–time finite element formulation to compute incompressible flows, including flows involving oscillating cylinders. One of the numerical examples considered in their study is flow past a cylinder which is subject to forced streamwise oscillations at $R = 100$ with symmetrical shedding ($A = 0.5$, $f/f_0 = 2.1$). Chang and Sa (1992) employed the Euler-explicit finite-difference scheme together with a stabilized error vector propagation method to simulate the flow past an oscillating cylinder. The simulations are conducted at $R = 100 : 0.1 \leqslant A \leqslant 0.4$ and $1.8 \leqslant f/f_0 \leqslant 2.4$, and the cylinder is allowed only harmonic motion in the streamwise direction. Sarpkaya et al. (1992) utilized a third-order in time, second-order in space, three-level predictor–corrector finite-difference scheme to compute the flow at $R = 800$ and sufficiently large amplitude. Graham et al. (1993) employed a vortex method and focused on relatively large amplitude and low-frequency oscillations using current speed to oscillatory velocity ratios between 0 and 5 at Reynolds numbers in the range $800 \leqslant R \leqslant 5200$. In these two-dimensional numerical investigations, only a short paper by Chang and Sa (1992) focused solely on the forced streamwise oscillation case.

The objective of this study is to numerically investigate the unsteady wake structures and lock-on phenomena in the near-wake region as well as the fluid forces at $R = 200 : A = 0.1$, 0.3 and $0.5 \leqslant f/f_0 \leqslant 3.0$. The near-wake vorticity contours and Lissajous patterns of unsteady lift coefficient are used to analyze the lock-on phenomenon following partly the methodology of Cetiner and Rockwell (2001). For comparison purposes the flow is calculated at $R = 855$, $A = 0.13$ and $f/f_0 = 2.0$, 3.0 and a series of numerical simulations are conducted in the stationary cylinder case at $R = 10^3$. Forcing a bluff body to oscillate introduces a mechanism for synchronizing the moment of shedding along its length. With this consideration, two-dimensional numerical simulations should be reliable in terms of analyzing flow details. To date, a detailed analysis of locked-on flow regimes, determined numerically, and analyzed in terms of near-wake vorticity contours and Lissajous patterns of unsteady lift coefficient has not been available. We intend to focus on this analysis in this study.

2. Methodology

A flow configuration of the present model is shown in Fig. 1. The nondimensional governing equations for the laminar two-dimensional motion of unsteady incompressible fluid are the Navier–Stokes equations together with the continuity equation in the noninertial reference frame which is attached to the cylinder. These equations in vorticity-stream-function formulation, after making use of the modified polar coordinates $(\xi, \theta) : \xi + \mathrm{i}\theta = \log(x + \mathrm{i}y)$, are

$$\mathrm{e}^{2\xi}\frac{\partial \zeta}{\partial t} = \frac{2}{R}\left(\frac{\partial^2 \zeta}{\partial \xi^2} + \frac{\partial^2 \zeta}{\partial \theta^2}\right) + \frac{\partial \psi}{\partial \xi}\frac{\partial \zeta}{\partial \theta} - \frac{\partial \psi}{\partial \theta}\frac{\partial \zeta}{\partial \xi}, \tag{1}$$

$$\frac{\partial^2 \psi}{\partial \xi^2} + \frac{\partial^2 \psi}{\partial \theta^2} = \mathrm{e}^{2\xi}\zeta, \tag{2}$$

where the domain of the problem is $D_{(\xi,\theta,t)} = \{(\xi, \theta, t) : 0 \leqslant \xi \leqslant \infty, 0 \leqslant \theta < 2\pi, t \geqslant 0\}$.

On the surface of the cylinder, the boundary conditions for velocity components are those of no-slip and impermeability conditions, i.e.,

$$\psi = \frac{\partial \psi}{\partial \xi} = 0 \quad \text{when } \xi = 0. \tag{3}$$

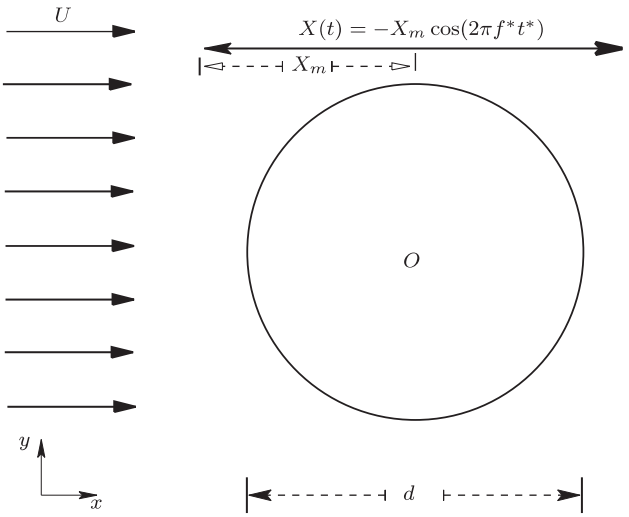

Fig. 1. The physical model and coordinate system.

At infinity, the boundary conditions are the free-stream condition and resulting decay of the vorticity. Mathematically, these conditions are presented, respectively, as

$$e^{-\xi}\frac{\partial\psi}{\partial\theta} \to (1+\dot{X}(t))\cos\theta \quad \text{as } \xi\to\infty, \tag{4}$$

$$e^{-\xi}\frac{\partial\psi}{\partial\xi} \to (1+\dot{X}(t))\sin\theta \quad \text{as } \xi\to\infty \tag{5}$$

and

$$\zeta \to 0 \quad \text{as } \xi\to\infty. \tag{6}$$

As a result of the coordinate system employed, the dependent variables ψ and ζ should be periodic functions of θ with period 2π, i.e.,

$$\zeta(\xi,\theta,t)=\zeta(\xi,\theta+2\pi,t), \quad \psi(\xi,\theta,t)=\psi(\xi,\theta+2\pi,t). \tag{7}$$

Boundary condition (6) gives a requirement for the vorticity in the far field, but there is no explicit condition for the vorticity on the surface of the cylinder at $\xi=0$. In this study, integral conditions are used to predict the surface vorticity. Following the work of Dennis and Quartapelle (1989) and Dennis and Kocabiyik (1991), the conditions on the stream function (4) and (5) are transformed into a set of global integral conditions on the vorticity using the continuity equation (2) and applying one of Green's identities to the flow domain. These integral conditions are given by

$$\int_0^\infty\int_0^{2\pi} e^{(2-p)\xi}\zeta(\xi,\theta,t)\cos(p\theta)\,d\theta\,d\xi = 0, \tag{8}$$

$$\int_0^\infty\int_0^{2\pi} e^{(2-p)\xi}\zeta(\xi,\theta,t)\sin(p\theta)\,d\theta\,d\xi = 2\pi(\dot{X}(t)+1)\delta_{p,1} \tag{9}$$

for $p=0,1,\ldots$, where $\delta_{p,j}$ is the Kronecker delta. Initial conditions for this set of equations will be addressed in the next section.

These integral conditions are used in a recent study by Kocabiyik et al. (2004) in the case of an asymmetric flow problem of an obliquely oscillating cylinder at an angle η to that of the uniform stream. In their work, when $\eta=0$, integral conditions reduce to (8) and (9). The use of integral conditions in symmetric flow problems can also be found [see, e.g., Badr et al. (1995)]. Badr et al. investigated a symmetrical flow induced by streamwise oscillations of a cylinder placed in a quiescent viscous fluid by using a single set of integral conditions which is similar to (9). Due to the correct numerical implementation of these conditions, the computed steady-state mean flow is found to be in excellent

agreement with the experiments of Tatsuno [see VanDyke (1982, p. 23)]. The present study represents an extension of that problem that takes into account the presence of a uniform background flow.

2.1. Numerical procedure

The numerical technique employed is due to Professor S.C.R. Dennis and has been successfully applied to simulations of flows past cylinders including oscillating and steadily rotating cylinders [see, e.g., Al-Mdallal (2004), Lawrence (2004) and the references cited therein]. Following the works of Collins and Dennis (1973a) and Badr and Dennis (1985), the stream function ψ and vorticity ζ are expressed as a truncated Fourier series of the form

$$\zeta(\xi,\theta,t) \simeq \frac{1}{2}G_0(\xi,t) + \sum_{n=1}^{N}[G_n(\xi,t)\cos(n\theta) + g_n(\xi,t)\sin(n\theta)], \tag{10a}$$

$$\psi(\xi,\theta,t) \simeq \frac{1}{2}F_0(\xi,t) + \sum_{n=1}^{N}[F_n(\xi,t)\cos(n\theta) + f_n(\xi,t)\sin(n\theta)], \tag{10b}$$

where N is the order of truncation. Substituting (10a,b) into (1) and (2), respectively, $4N+2$ interdependent ordinary differential equations given by

$$e^{2\xi}\frac{\partial G_0}{\partial t} = \frac{2}{R}\frac{\partial^2 G_0}{\partial \xi^2} + \sum_{m=1}^{N} m\frac{\partial}{\partial \xi}(F_m g_m - f_m G_m), \tag{11a}$$

$$e^{2\xi}\frac{\partial G_n}{\partial t} = \frac{2}{R}\left(\frac{\partial^2 G_n}{\partial \xi^2} - n^2 G_n\right) - \frac{1}{2}nf_n\frac{\partial G_0}{\partial \xi} + \frac{1}{2}S_n, \tag{11b}$$

$$e^{2\xi}\frac{\partial g_n}{\partial t} = \frac{2}{R}\left(\frac{\partial^2 g_n}{\partial \xi^2} - n^2 g_n\right) + \frac{1}{2}nF_n\frac{\partial G_0}{\partial \xi} + \frac{1}{2}T_n, \tag{11c}$$

$$\frac{\partial^2 F_0}{\partial \xi^2} = e^{2\xi}G_0, \quad \frac{\partial^2 F_n}{\partial \xi^2} - n^2 F_n = e^{2\xi}G_n, \quad \frac{\partial^2 f_n}{\partial \xi^2} - n^2 f_n = e^{2\xi}g_n, \tag{12a,b,c}$$

are obtained, where

$$S_n = \sum_{m=1}^{N}\left\{[(m-n)F_k + lF_l]\frac{\partial g_m}{\partial \xi} - [kf_k + lf_l]\frac{\partial G_m}{\partial \xi} + mg_m\left[\frac{\partial F_k}{\partial \xi} + \frac{\partial F_l}{\partial \xi}\right] - mG_m\left[\mathrm{sgn}(m-n)\frac{\partial f_k}{\partial \xi} + \frac{\partial f_l}{\partial \xi}\right]\right\}, \tag{13}$$

and

$$T_n = \sum_{m=1}^{N}\left\{[lf_l - kf_k]\frac{\partial g_m}{\partial \xi} - [(m-n)F_k - lF_l]\frac{\partial G_m}{\partial \xi} - mG_m\left[\frac{\partial F_k}{\partial \xi} - \frac{\partial F_l}{\partial \xi}\right] - mg_m\left[\mathrm{sgn}(m-n)\frac{\partial f_k}{\partial \xi} - \frac{\partial f_l}{\partial \xi}\right]\right\} \tag{14}$$

for all integers $1 \leqslant n \leqslant N$ with $k = |m-n|$ and $l = m+n$. Here, f_0 and g_0 are assumed identically zero. The boundary conditions associated with Eqs. (11) and (12) follow directly from (3), (6), (8) and (9). They are

$$F_n = f_n = \frac{\partial F_n}{\partial \xi} = \frac{\partial f_n}{\partial \xi} = 0 \quad \text{at } \xi = 0, \tag{15}$$

$$\int_0^\infty e^{(2-n)\xi}G_n(\xi,t)\,d\xi = 0, \quad \int_0^\infty e^{(2-n)\xi}g_n(\xi,t)\,d\xi = 2(\dot{X}(t)+1)\delta_{n,1}, \tag{16}$$

$$G_n(\xi,t) = g_n(\xi,t) = 0 \quad \text{as } \xi \to \infty \tag{17}$$

for $n = 0,1,2,\ldots,N$ and $t > 0$.

The domain of these equations in the physical coordinate system is given by $D_{(\xi,t)} = \{(\xi,t) : \xi \in [0,\infty), t > 0\}$. The initial conditions for these equations are not immediately available. Thus, boundary-layer theory for impulsively started flows is used to provide initial conditions by introducing the boundary-layer coordinate z through the transformation

$$\xi = kz, \tag{18}$$

where $k=(8t/R)^{1/2}$ [see, e.g., Schlichting (2000)]. An order of magnitude analysis shows that ψ and ζ scale using k as follows:

$$\psi = k\Psi, \quad \zeta = \omega/k. \tag{19}$$

Consequently, Eqs. (11b,c) and (12b,c) can be rewritten, respectively, in final form for small values of k, $k \leqslant 1$, as

$$4t\frac{\partial G_n}{\partial t} = \mathrm{e}^{-2kz}\frac{\partial^2 G_n}{\partial z^2} + 2z\frac{\partial G_n}{\partial z} + (2-n^2k^2\mathrm{e}^{-2kz})G_n - 2t\mathrm{e}^{-2kz}\left(n\frac{\partial G_0}{\partial z}f_n - S_n\right), \tag{20}$$

$$4t\frac{\partial g_n}{\partial t} = \mathrm{e}^{-2kz}\frac{\partial^2 g_n}{\partial z^2} + 2z\frac{\partial g_n}{\partial z} + (2-n^2k^2\mathrm{e}^{-2kz})g_n + 2t\mathrm{e}^{-2kz}\left(n\frac{\partial G_0}{\partial z}F_n + T_n\right), \tag{21}$$

$$\frac{\partial^2 F_n}{\partial z^2} - n^2k^2F_n = \mathrm{e}^{2kz}G_n, \quad \frac{\partial^2 f_n}{\partial z^2} - n^2k^2f_n = \mathrm{e}^{2kz}g_n, \tag{22,23}$$

where the domain $D_{(\xi,t)}$ is transformed to $D_{(z,t)} = \{(z,t) : z \in [0,\infty),\ t>0\}$. Here S_n and T_n are as before with ξ replaced by z.

The boundary conditions that are associated with Eqs. (21) and (22) can be obtained easily from the boundary conditions (15)–(17). The initial conditions at $t=0$ can be determined exactly following the methodology of Collins and Dennis(1973b) and Badr and Dennis (1985). These conditions at time $t=0$ are given by

$$G_n(z,0)=0, \quad g_n(z,0)=\frac{4\,\mathrm{e}^{-z^2}}{\sqrt{\pi}}\delta_{n,1}, \quad F_n(z,0)=0, \quad f_n(z,0)=-2\left(\frac{1-\mathrm{e}^{-z^2}}{\sqrt{\pi}} - z\,\mathrm{erf}(z)\right)\delta_{n,1} \tag{24}$$

for all $z \in [0,\infty)$.

The numerical solution of the set of equations both in boundary-layer and in physical coordinates has been discussed in detail by Collins and Dennis (1973a) and Badr and Dennis (1985). Since the computational domain in the spatial, z and ξ, directions is unbounded, a large enough artificial outer boundary, z_∞ and ξ_∞, respectively, must be chosen to represent infinity for the numerical treatment. The solution through time domain is then divided into two distinct zones:

$$(0,\ t_s] \quad \text{and } (t_s,\ t_{\max}],$$

where t_s represents the switching time from the boundary-layer coordinate, z, to the physical coordinate, ξ, and $t_{\max}$ represents the time at the end of the calculations. The solution in the first zone begins following the start of fluid motion and continues until the boundary-layer becomes thick enough to use physical coordinates at $t=t_s$ (i.e., $k_s=(8t/R)^{1/2}<1$). In the second zone where the boundary-layer coordinate, z, is replaced by the physical coordinate, ξ, the integration starts at $t=t_s^+$ and continues until the termination of calculations at $t=t_{\max}$. For the vorticity components (G_0, G_n or g_n), the implicit Crank–Nicolson scheme is used to advance the solution a single time step to $t=t_{j+1}$. The central finite-difference formula is used to approximate derivatives with respect to the spatial coordinates, z and ξ. The numerical solution for the corresponding stream function components F_n and f_n is obtained using stable integration procedures given by Dennis and Chang (1969) and Badr and Dennis (1985). The Gauss–Seidel iterative method is incorporated to obtain a solution consistent for the full system. The convergence criterion is achieved when the difference between two successive iterations of all the calculated solutions falls below the specified tolerance of $\varepsilon=10^{-6}$.

In order to implement this numerical scheme correctly, careful attention is given to the selection of the numerical parameters $N, t_s, z_\infty, \xi_\infty$ as well as the time steps Δt_{j+1} and spatial steps h_z and h_ξ in both the boundary-layer and physical coordinates ((z,t); (ξ,t)), respectively. The uniform grids h_z and h_ξ should be chosen to be consistent with z_∞ and ξ_∞, respectively. Furthermore, numerical simulations suggest that choosing $t_s=20$, so that $k_s<1$, provides accurate results for the range of parameters considered. The "optimal" values for the remaining parameters are determined by conducting simulations for each choice of flow parameters with the exception of the order of truncation of the Fourier expansion which is arranged automatically. Initially there are two terms. Then, one more term is added when the last term exceeds 10^{-3} with the maximum number of terms $N=60$. The rapid variation of vorticity near $t=0$ requires the use of a small time step initially. The time step is chosen as $\Delta t_{j+1}=10^{-3}$ for the first 10 steps, and then it is increased to $\Delta t_{j+1}=10^{-2}$ for the rest of the calculations. The grid size in the z-direction is taken as $h_z=0.025$ and the artificial boundary z_∞ is restricted to 8.

Numerical simulations via C++ are carried out on a 64-processor Beowulf cluster located in the Department of Mathematics and Statistics, and on a Silicon Graphics (SGI) Onyx 3400 computer, which has 28 400 MHz IP35 MIPS

R12000 processors, located in the Advanced Computation and Visualization Centre, both at Memorial University of Newfoundland.

2.2. Force calculation

The fluid forces exerted on the cylinder surface are represented by the dimensionless drag and lift coefficients, defined as

$$C_D = \frac{D}{\frac{1}{2}\rho U^2 d}, \quad C_L = \frac{L}{\frac{1}{2}\rho U^2 d}, \tag{25}$$

where D and L are the drag and lift forces exerted on a unit length of the cylinder, respectively; and ρ is the fluid density. The final expressions, after integrating the normal and shear stresses around a closed contour that contains the cylinder (or Stoke's relations), are

$$C_D = \frac{D}{\frac{1}{2}\rho U^2 d} = \frac{2}{R}\int_0^{2\pi} \zeta|_{\xi=0} \sin\theta \, \mathrm{d}\theta - \frac{2}{R}\int_0^{2\pi} \left.\frac{\partial\zeta}{\partial\xi}\right|_{\xi=0} \sin\theta \, \mathrm{d}\theta - \pi\ddot{X}(t), \tag{26a}$$

$$C_L = \frac{L}{\frac{1}{2}\rho U^2 d} = -\frac{2}{R}\int_0^{2\pi} \zeta|_{\xi=0} \cos\theta \, \mathrm{d}\theta + \frac{2}{R}\int_0^{2\pi} \left.\frac{\partial\zeta}{\partial\xi}\right|_{\xi=0} \cos\theta \, \mathrm{d}\theta. \tag{26b}$$

The first integral in each expression of (26a) represents the coefficient due to friction and the second terms are due to pressure. Further, the term $-\pi\ddot{X}(t)$ appearing in the drag coefficient is a result of the acceleration due to time-dependent cylinder oscillation.

2.3. Validation

The reliability of the mathematical model as well as the accuracy of the present method are presented for uniform flow past a stationary cylinder and a cylinder undergoing forced streamwise oscillations in a uniform free-stream. As is well known, if unaltered, any numerical method [see, e.g., Braza et al. (1986)] produces symmetric vortices behind the cylinder for all times, for the mathematical models used to describe these cases, although the physical flows are asymmetric. This behavior results from the fact that, at any instant, the total speed of the upper and lower parts of the cylinder (and thus the behavior of fluid in these regions) are exactly the same, as a result of the symmetric boundary conditions imposed on the flow. However, physically realistic flows of this type are not symmetric and thus a velocity gradient must exist for the fluid on the cylinder surface. Taking this into account, an artificial perturbation is imposed to break this perfect numerical symmetry, which is similar to that reported in previous studies (Martinez and Hinh, 1978; Braza et al., 1986; Justesen, 1991) in which a clockwise rotation of the circular cylinder was followed after a short period of time by a counterclockwise rotation. Following the work of Braza et al. (1986), a perturbation is implemented with dimensionless angular displacement given by

$$\Theta(t) = -\frac{\pi}{4}\cos\left(\frac{2\pi}{5}t\right) \tag{27}$$

for a full period of rotational oscillation.

The drag coefficient for the case of uniform flow past a stationary cylinder at $R = 10^3$ is compared with the results of Cheng et al. (1997), Koumoutsakos and Leonard (1995), and Qian and Vezza (2001) in Fig. 2 [reproduced from Lawrence (2004)]. In each of these studies, a different numerical scheme is used to integrate the governing equations. The instantaneous streamlines at dimensionless time $t = 2.5$ are also given in Fig. 3 [reproduced from Lawrence (2004)]. From these figures it is apparent that our numerical scheme can accurately predict the flow from the beginning of the calculations. To compare with the experimental findings of Ongoren and Rockwell (1988), numerical simulations are performed at $R = 855$ for uniform flow past a cylinder subject to streamwise oscillations. Fig. 4 [reproduced from Al-Mdallal (2004)] shows the comparison of the near-wake structure obtained in the present study when $R = 855$, $A = 0.13$ and $f/f_0 = 2.0$, 3.0 with that obtained by Ongoren and Rockwell (1988). It should be noted that the number of oscillation cycles for the experimental trials of Ongoren and Rockwell (1988) is considerably higher than that of the present case. Nonetheless, there is remarkable agreement between our computed near-wake structures and those shown in the experimental images.

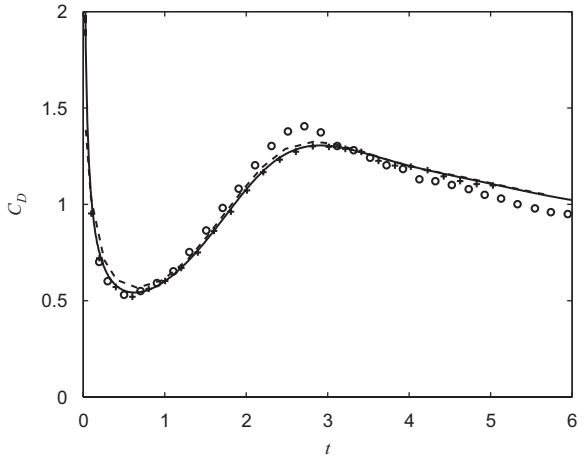

Fig. 2. Comparison of drag coefficient for the case of uniform flow past a stationary cylinder at $R = 10^3$: —, present; ○, Cheng et al. (1997); +, Koumoutsakos and Leonard (1995); − −, Qian and Vezza (2001).

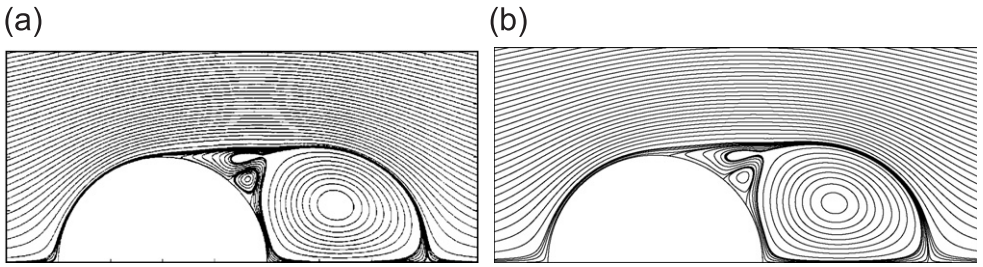

Fig. 3. Comparison of streamline patterns for the case of uniform flow past a stationary cylinder at $R = 10^3$: (a) Qian and Vezza (2001); (b) present.

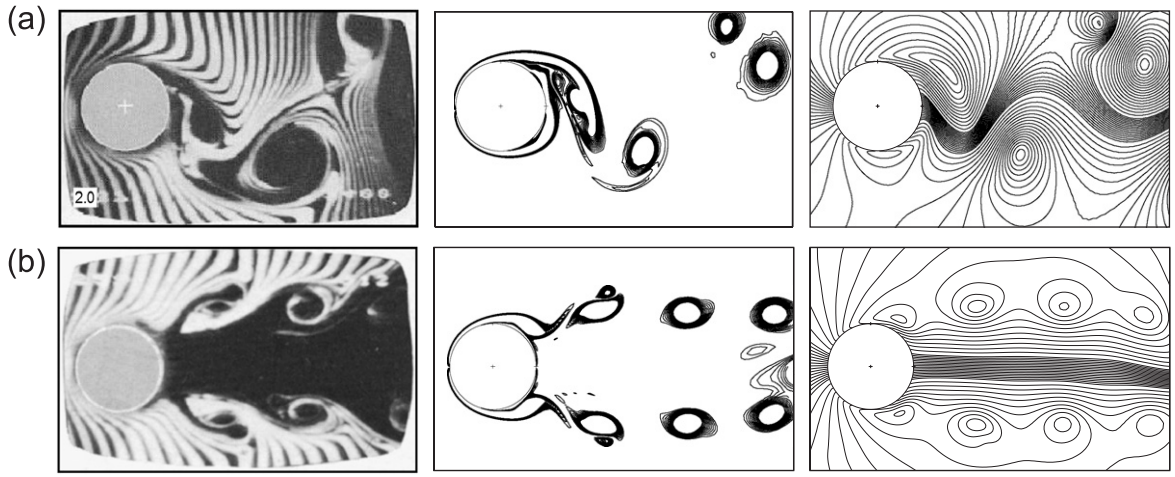

Fig. 4. Comparison of Left: flow visualization of Ongoren and Rockwell (1988); Middle: computed present equivorticity lines; Right: streamline patterns for $R = 855$, $A = 0.13$ at frequency ratios. (a) $f/f_0 = 2.0$; (b) $f/f_0 = 3.0$. All snapshots are taken at the instant corresponding to the maximum negative displacement.

3. Results and discussion

The present numerical simulations confirmed two basic groups of asymmetric and symmetric modes of vortex formation in the near-wake region which have been consistently observed in several previous studies [see, e.g., Ongoren and Rockwell (1988), Lecointe and Piguet (1989)]. There is a single symmetric vortex pair mode and there are three basic asymmetric modes, 2S, S+P and 2P, where S and P indicate a 'single' vortex and a 'pair' of shed vortices, respectively, as described in the introduction section. A single vortex-shedding cycle, T_v, is defined as the time interval required to complete one cycle of vortex shedding and it is related to the cylinder oscillation period, $T(=1/f)$, by $T_v = n\ T$: n either fraction or integer number. We note that increasing the forcing frequency and oscillation amplitude beyond a certain value results in the formation of secondary vortices adjacent to the dominant vortices being shed, but these vortices coalesce very close to the cylinder, before the secondary vortices obtain a clearly defined center. These vortices will not be used in the classification process. We use the terminology of Williamson and Roshko (1988) from their transverse forced experiments to categorize vortex formation modes resulting from forced streamwise cylinder oscillation in the near-wake region. This is consistent with streamwise mode classification reported in the literature [see, e.g., Jauvtis and Williamson (2004), Konstantinidis et al. (2005)]. However, Ongoren and Rockwell (1988) classified (i) symmetric vortex pair mode (per T) as "*the symmetric S mode*" and (ii) asymmetric modes: 2S (per T), 2S (per $2T$), S+P (per $2T$) and 2P (per $2T$) as "*the asymmetric AI, AII, AIII and AIV modes*", respectively. In classifying these modes, only the near-wake region is considered by Ongoren and Rockwell, whereas Williamson and Roshko consider the entire wake of the cylinder and are not concerned with these near-field formations. Moreover, Ongoren and Rockwell (1988) noted that under certain conditions a mirror image of the near-wake pattern, which can persist for 50 or more cycles of oscillation, is formed if the flow is stopped and restarted. This is one example of the complexity of the flow patterns which accompany the oscillations. For example, when $f = 2f_0$ the oscillation and vortex frequencies are phase locked, but under other nonresonant conditions there is competition between the symmetric and asymmetric modes. Under these conditions, the lock-on persists in one mode over a specified number of cycles and then switches to other mode. The mode competition is influenced by the upstream feedback of disturbances from the near-wake of the cylinder. In our numerical study when different types of perturbations are used, a mirror image of the mode 2S per $2T$ is formed.

A more general approach for categorizing the vortex-shedding modes is taken by Zdravkovich (1996) in which vortex shedding from a cylinder is classified as either in a low-speed mode or a high-speed mode. The low speed is related to laminar wake instability whereas the high-speed mode is related to vortex formation and shedding. The transition between these two states is characterized by distortions of eddy filaments in the near-wake, referred to as 'fingers' which

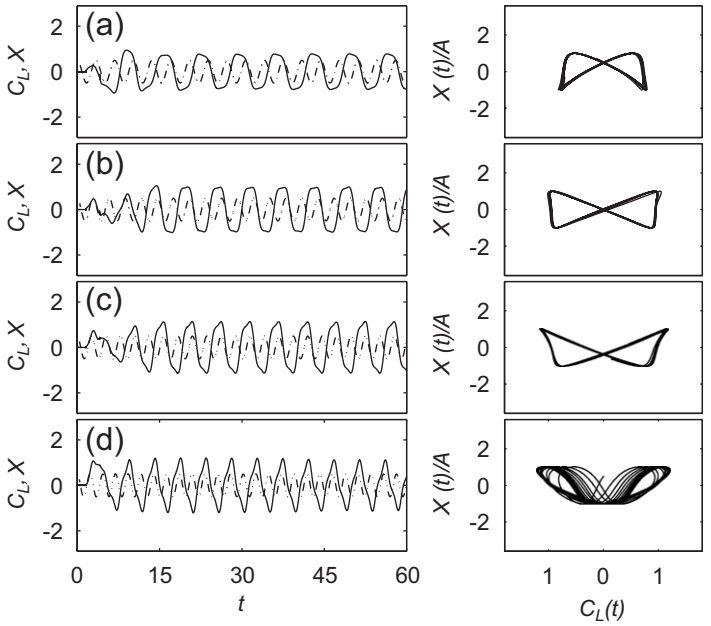

Fig. 5. Left: —, the time variation of the lift coefficient, $C_L(t)$; —•—, streamwise displacement, $X(t)$ and Right: the Lissajous patterns, $X(t)/A$ versus $C_L(t)$ for $R = 200$, $A = 0.1$. (a) $f/f_0 = 1.5$, (b) $f/f_0 = 1.75$, (c) $f/f_0 = 1.95$, (d) $f/f_0 = 2.2$.

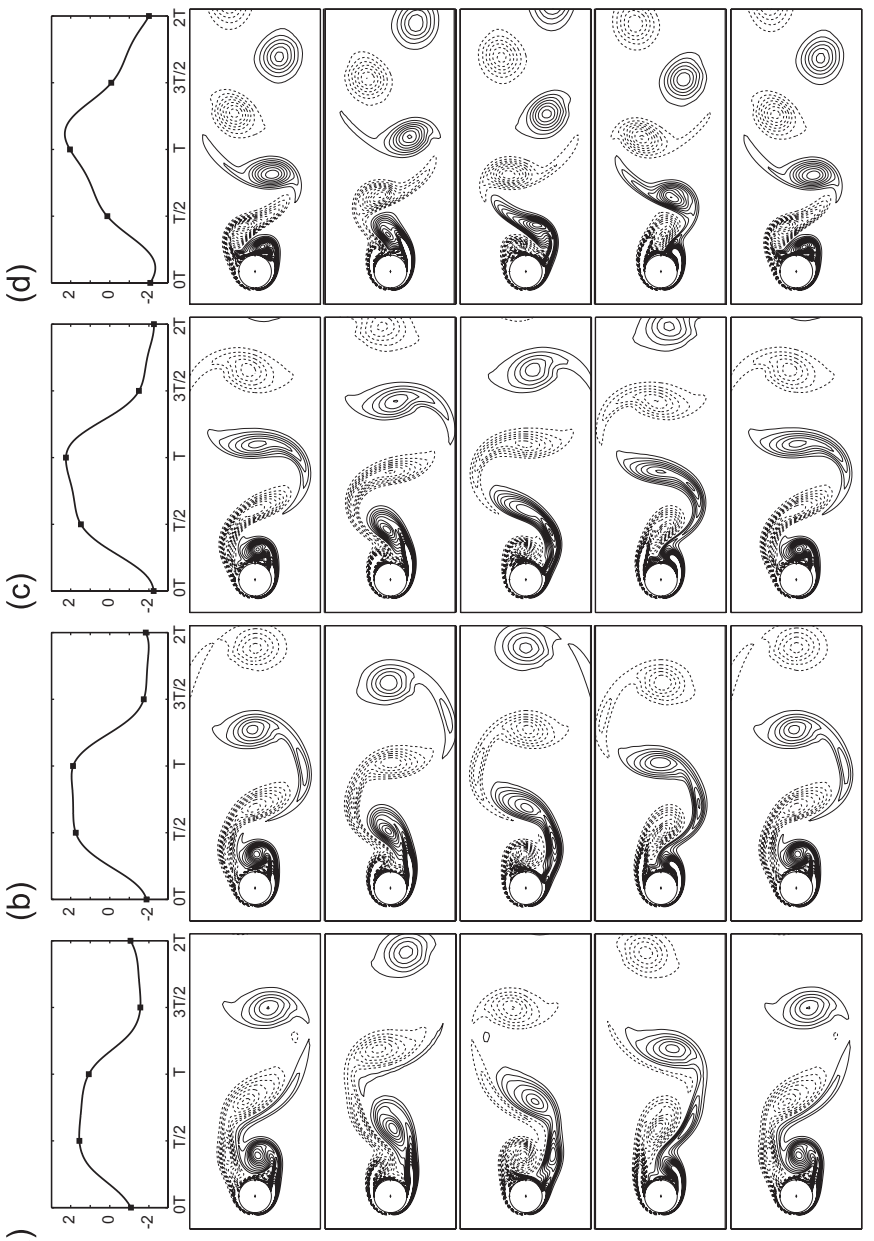

Fig. 6. Equivorticity lines over two periods of oscillation, $2T$, for $R = 200$, $A = 0.1$: (a) $f/f_0 = 1.5$; (b) $f/f_0 = 1.75$; (c) $f/f_0 = 1.95$; (d) $f/f_0 = 2.2$. The instantaneous snapshots are marked in the corresponding lift coefficient curve shown above the snapshots for each frequency.

cause irregular vortex filaments to appear along the span. Zdravkovich (1996) also described two modes in the streamwise oscillation of a cylinder near the synchronization frequency: one vortex formed per half-cycle and two vortices formed per half-cycle. The transition state from the first mode to the second mode is characterized by one vortex formed in odd half-cycles and two vortices formed in even half-cycles.

Finally, it is noted that the classical definition of locked-on flow regimes is based on the existence of a dominant peak in the power spectral density of the lift coefficient. However, the determination of locked-on flow regimes is not confined to the power spectral density analysis of the lift records. For instance, Anagnostopoulos (2000) uses the power spectral density analysis or repetition of the velocity traces to classify locked-on modes and Ongoren and Rockwell (1988) classify lock-on regimes based on a repetition of vortex shedding in the near-wake region over an integer number of cylinder oscillation periods. In this study, locked-on flow regimes are analyzed in terms of near-wake vorticity contours and Lissajous patterns of unsteady lift coefficient, following partly the methodology of Cetiner and Rockwell (2001). The main calculations are performed at $R = 200$ and $A = 0.1,\ 0.3$ while the frequency ratio f/f_0 varies from 0.5 to 3 by increments of 0.05. Only those cases necessary to support claims are presented. For comparison purposes, the flow is also calculated at $R = 855$, $A = 0.13$ and $f/f_0 = 2.0, 3.0$, and a series of numerical simulations are conducted in the stationary cylinder case at $R = 10^3$, as shown in Validation section. Predicted values for f_0 at $R = 200, 855$ are $0.195, 0.22$, respectively, and they are calculated using the power spectral density of the lift coefficient for the case of uniform flow past a stationary circular cylinder.

3.1. Amplitude $A = 0.1$

The case for $R = 200$ and $A = 0.1$ is first considered. The time history of the fluctuating lift coefficients up to nondimensional time $t = 60$ (left) and the corresponding Lissajous patterns (i.e., $X(t)/A$ versus $C_L(t)$) (right) are shown in Fig. 5 for $1.5 \leqslant f/f_0 \leqslant 2.2$. It is clear that the cylinder excitation in all cases produces a repetitive signature of the lift coefficient every two cycles of cylinder oscillation, $2T$, which is also suggested by the corresponding Lissajous pattern. These observations suggest that the vortex shedding in the near-wake region is locked-on over two periods, $2T$. Fig. 6 displays typical equivorticity patterns for $f/f_0 = 1.5, 1.75, 1.95, 2.2$ over two periods of cylinder oscillation with the corresponding excerpt from the lift coefficient displayed above. The snapshots are taken at the instant $X(t) = A$ and every half oscillation cycle thereafter as marked by the boxes on the lift curves. As will be the case in all equivorticity plots that follow, positive contours are indicated by solid lines and negative contours by dashed lines. The snapshots at $t = 0$ (top) and $t = 2T$ (bottom) for all cases are nearly identical. Therefore, the lock-on occurs over a span of frequency that brackets twice the natural shedding frequency given by $f/f_0 \in [1.5, 2.2]$. In this range, the pronounced decrease of vortex formation length as f/f_0 increases from 1.5 to 2.2 causes the disappearance of the second weaker vortex from each side of the cylinder. Consequently, the locked-on asymmetric 2P, mode per $2T$ is observed for $1.5 \leqslant f/f_0 \leqslant 2.0$ and the locked-on asymmetric 2S mode per $2T$ for $2.0 < f/f_0 \leqslant 2.2$. In the 2P mode, the second weaker vortex of each pair vanishes downstream at or before a distance d measured from the trailing edge of the cylinder. However, it is observed that for $f/f_0 \leqslant 1.85$ this smaller vortex decays, whereas for $f/f_0 > 1.85$ it coalesces with the larger vortex (another result of the shortening formation length). This noted decrease in the formation length is well documented in the visualizations of Ongoren and Rockwell (1988) at different flow parameters. Investigation of the lift coefficient (see Fig. 7) and the structure of the near-wake region at $f/f_0 = 2.8$ leads to the locked-on behavior shown in Fig. 8. Typical equivorticity and streamline visualizations as well as the lift coefficient display a quasi-periodic pattern every three periods of cylinder oscillation ($3T$), referred to as 'tertiary' lock-on. In this mode, three vortices develop on each side of the cylinder over three periods of cylinder, oscillation yielding a total of six shed vortices. The three vortices shed from

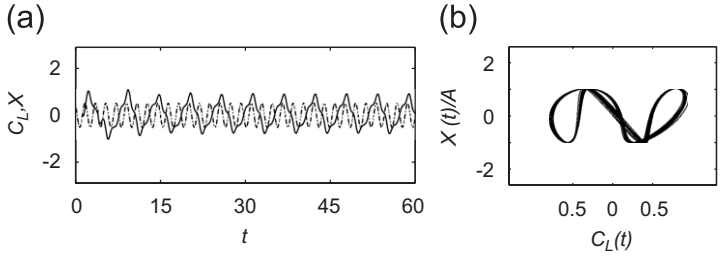

Fig. 7. (a) —, The time variation of the lift coefficient, $C_L(t)$; —•—, streamwise displacement, $X(t)$; (b) the Lissajous patterns, $X(t)/A$ versus $C_L(t)$; for $R = 200$, $A = 0.1$: $f/f_0 = 2.8$.

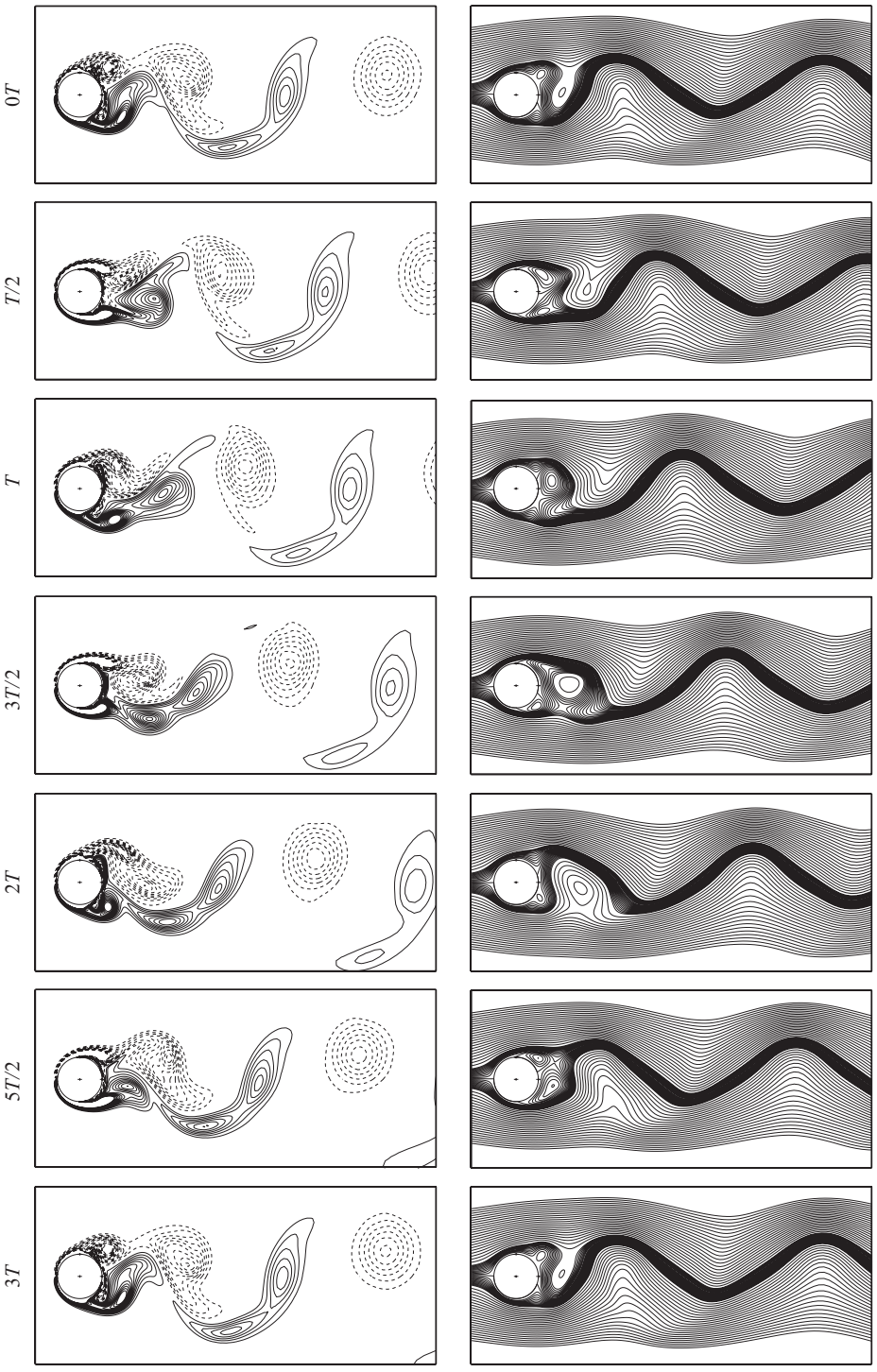

Fig. 8. Equivorticity lines over three periods of oscillation, $3T$, for $R = 200$, $A = 0.1$: $f/f_0 = 2.8$ ($T \approx 1.83$, $40.21 \leqslant t \leqslant 45.7$).

the upper side of the cylinder immediately coalesce in the near-wake region to form a single large vortex. In contrast, only two of three vortices developing on the bottom side of the cylinder coalesce, while the third vortex remains detached. Consequently, this mode of vortex formation is referred to as the asymmetric $6S \rightarrow P + S$ mode per $3T$. In

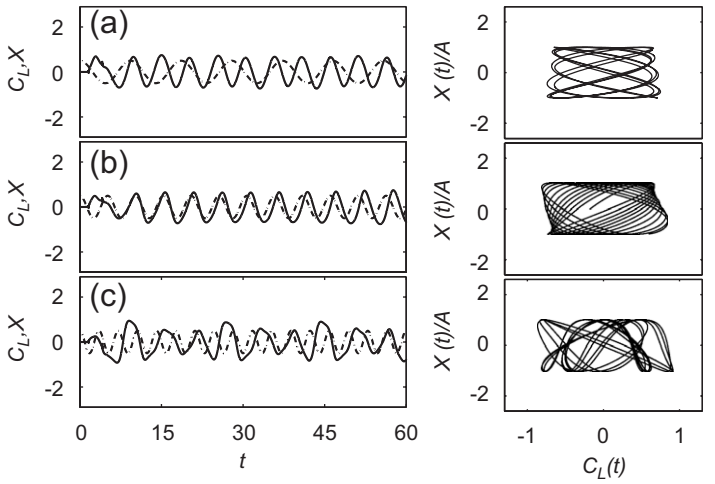

Fig. 9. Left: —, the time variation of the lift coefficient, $C_L(t)$; —•—, streamwise displacement, $X(t)$ and Right: the Lissajous patterns, $X(t)/A$ versus $C_L(t)$ for $R = 200$, $A = 0.1$. (a) $f/f_0 = 0.55$, (b) $f/f_0 = 1.0$, (c) $f/f_0 = 1.45$.

this manner the dynamics of the mode before (6S) and after (P + S) coalescence, respectively, are described effectively. This phenomenon is not observed for any other values of the forcing frequency.

Lock-on is not observed at any other frequency ratio in $0.5 \leqslant f/f_0 \leqslant 3.0$. Fig. 9 displays the lift and Lissajous curves for selected values of cylinder excitation frequency ($f/f_0 = 0.55$, 1.0 and 1.45) outside of the lock-on ranges discussed. Neither of these curves show a phase-locked pattern which is indicative of lock-on. At $f/f_0 = 1.0$, the lift pattern is nearly locked-on but it is concluded that it has not yet locked-on to the cylinder oscillation frequency. To support this claim, Fig. 10 displays a series of instantaneous equivorticity contours over 11 forcing periods. The snapshots are taken at the instant $X(t) = A$, and every full cycle of oscillation thereafter as indicated on the lift curve in the upper-left corner of the figure. It is evident from this figure that the near-wake frequency is not locked-on to the cylinder oscillation frequency.

The effect of the frequency ratio, f/f_0, on the lift and drag coefficients is displayed in Fig. 11. The maximum lift coefficient, $C_{L,\max}$, and time-averaged drag coefficient, $\bar{C}_D$, display a significant peak within the synchronization range, reaching a maximum near 2.0. The increase of both $C_{L,\max}$ and $\bar{C}_D$ within this lock-on range has been reported by Hurlbut et al. (1982), Clift et al. (1978), and others. The drag coefficient, C_D, oscillates at the forcing frequency, f, in-phase with the cylinder displacement, X, as a result of the purely horizontal motion. As the cylinder oscillation frequency increases, the maximum drag coefficient $C_{D,\max}$ increases and the minimum drag coefficient $C_{D,\min}$ decreases yielding a successive increase in the amplitude of the drag coefficient, $C_{D,\text{amp}}$.

In summary, for the low-amplitude case the vortex-shedding at the considered values of the forcing frequencies is characterized by asymmetric modes in the near-wake region. Furthermore, an increase of the $C_{L,\max}$ and $\bar{C}_D$ within the fundamental lock-on frequency range ($f/f_0 \approx 2$) is observed.

3.2. *Amplitude* $A = 0.3$

Fig. 12 displays the lift coefficients and corresponding Lissajous patterns for selected values of the forcing frequency from $f/f_0 = 1.1$ to $f/f_0 = 3.0$ when $R = 200$ and $A = 0.3$. This figure indicates that the lift has a repetitive behavior every two cycles of oscillation when $f/f_0 \in [1.1, 1.8]$, suggesting the existence of an asymmetric vortex-shedding mode. The amplitude of the lift coefficients seems damped when $f/f_0 \in [1.85, 3]$, a characteristic of a symmetric vortex-shedding mode. Hence, locked-on flow at $A = 0.3$ is found to occur within the frequency ratio range of [1.1, 3.0], a much larger range than found at $A = 0.1$.

Fig. 13 shows typical equivorticity patterns for $f/f_0 = 1.10$, 1.30, 1.40, 1.50 and 1.80 over two periods of cylinder oscillation, with snapshots taken at $X(t) = A$ and every half-cycle thereafter.The locked-on asymmetric modes 2P per $2T$ when $f/f_0 \in [1.1, 1.25]$, P + S per $2T$ when $f/f_0 \in [1.30, 1.75]$ and 2S per $2T$ when $f/f_0 = 1.8$ are verified in this figure. At $f/f_0 = 1.1 - 1.25$ the formation of the vortices just behind the cylinder appears to be P + S with the single vortex being shed from the bottom of the cylinder. The formation length for this vortex is long and it is observed that the shed layer remains in the near-wake during the shedding of the top vortices. The larger of the two vortices being

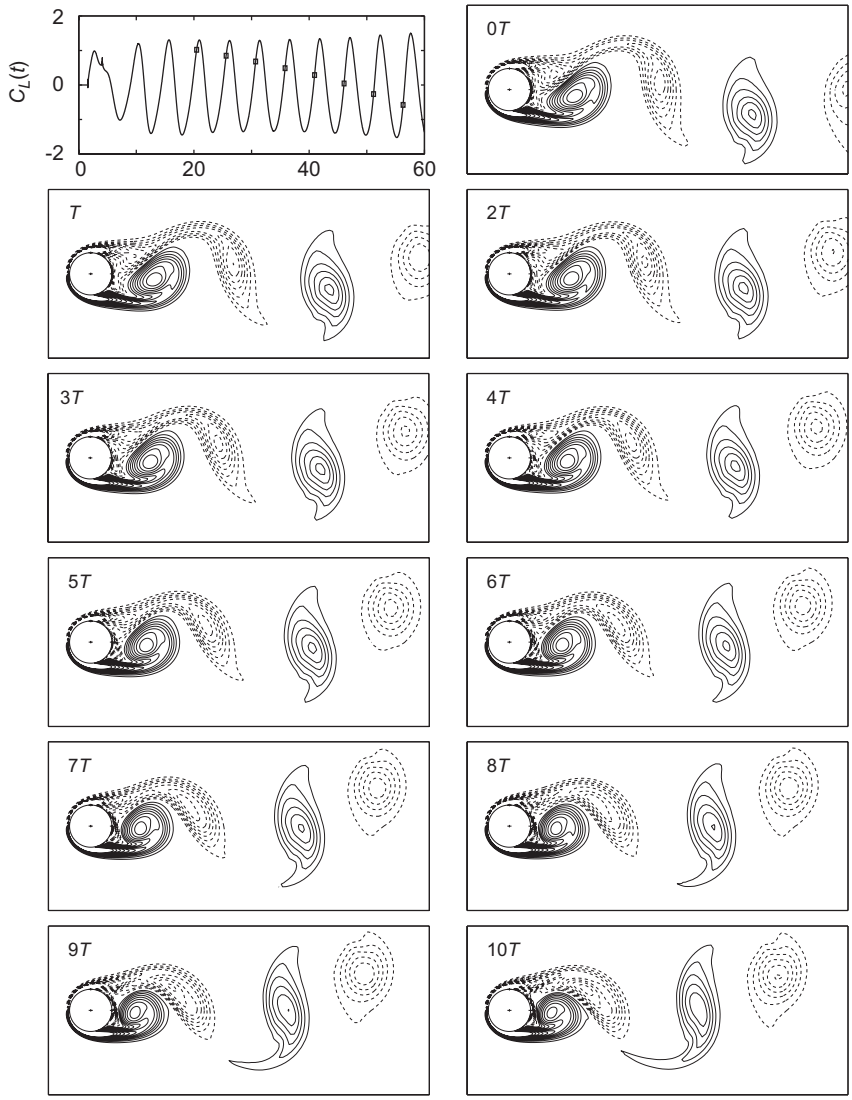

Fig. 10. Equivorticity lines at an instant corresponding to the maximum positive displacement over 10 periods of oscillations, $10T$, for $R = 200$, $A = 0.1$, $f/f_0 = 1.0$ (non-phase-locked regime). The instantaneous snapshots are marked in the corresponding lift coefficient curve.

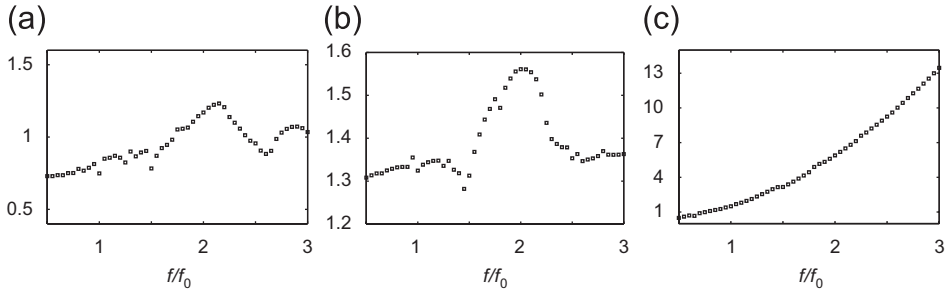

Fig. 11. Effect of f/f_0 on (a) $C_{L,\max}$; (b) $\bar{C}_D$; (c) $C_{D,\text{amp}}$, when $R = 200$, $A = 0.1$.

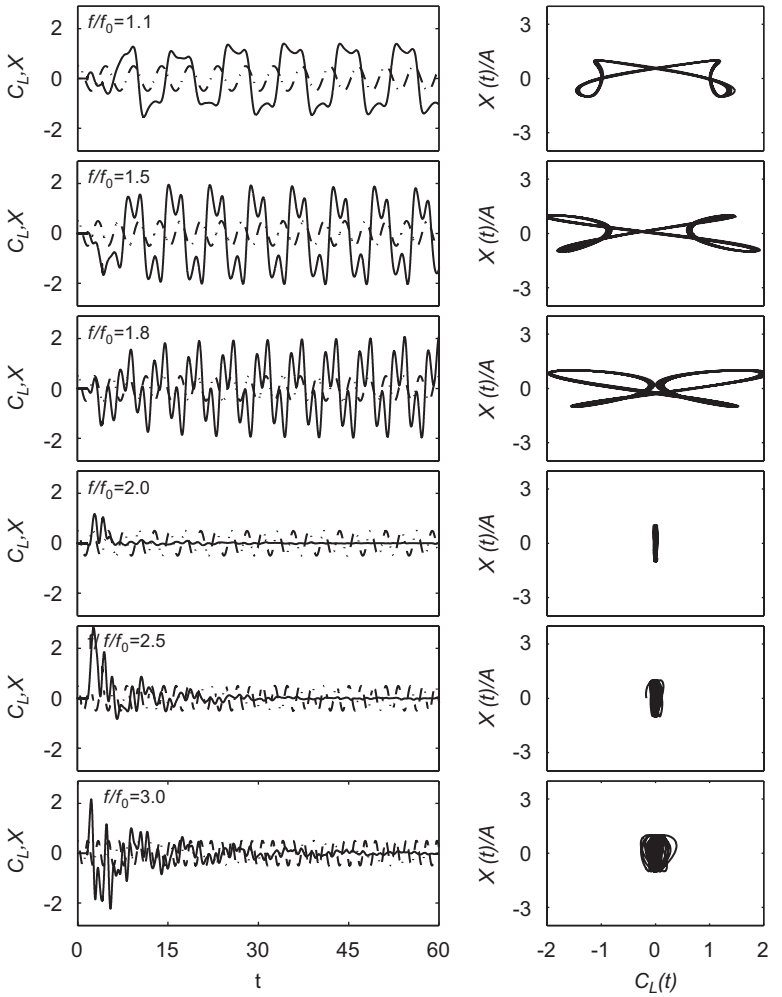

Fig. 12. Left: —, the time variation of the lift coefficient, $C_L(t)$; –•–, streamwise displacement, $X(t)$ and Right: the Lissajous patterns, $X(t)/A$ versus $C_L(t)$ for $R = 200$, $A = 0.3$: $1.1 \leqslant f/f_0 \leqslant 3.0$.

shed from the top has opposite rotation to its counterpart being shed from the bottom. As a result the fluid which would have just dissipated in the shed layer under ordinary circumstances begins to recirculate, creating a second weaker vortex on the bottom of the cylinder, and hence the 2P mode in this range of frequencies. This phenomenon is most pronounced at $f/f_0 = 1.25$ where the 2P mode has completely developed in the wake. The shortening of vortex formation length at $f/f_0 = 1.3$ and resultant strengthening of the bottom vortex diminishes the effect of the top vortices, yielding the P+S mode for further values of the forcing frequency up to $f/f_0 = 1.8$. At $f/f_0 = 1.8$, the formation length has shortened so much that the large vortex shedding from the bottom of the cylinder is causing the first vortex on the top to appear elongated and weakened. As a result, although remnants of the P+S in the near-wake are still observed, the transition is certainly towards the asymmetric 2S mode which is evident shortly downstream. At $f/f_0 = 1.8$, it is also noted that the near-wake structure shows a quasi-periodic pattern every $T/2$ (i.e., snapshots every $T/2$ are mirror images of one another). For $1.85 \leqslant f/f_0 \leqslant 3.0$, the vortex-shedding patterns display a synchronized symmetric vortex pair mode per T as seen in Fig. 14. In the figure, a pair of vortices are simultaneously shed from each side of the cylinder during one oscillation cycle which preserve their symmetry for a long distance downstream. Each of these large vortices is accompanied by a smaller counter-rotating vortex which quickly decays before moving downstream, a finding which is consistent with the experimental results of Ongoren and Rockwell (1988, p. 229). The appearance of these secondary vortices is attributed to the instability of flow in the shear layer around the cylinder. As a result of this symmetry, irrotational fluid is drawn along the wake centerline towards the cylinder base.

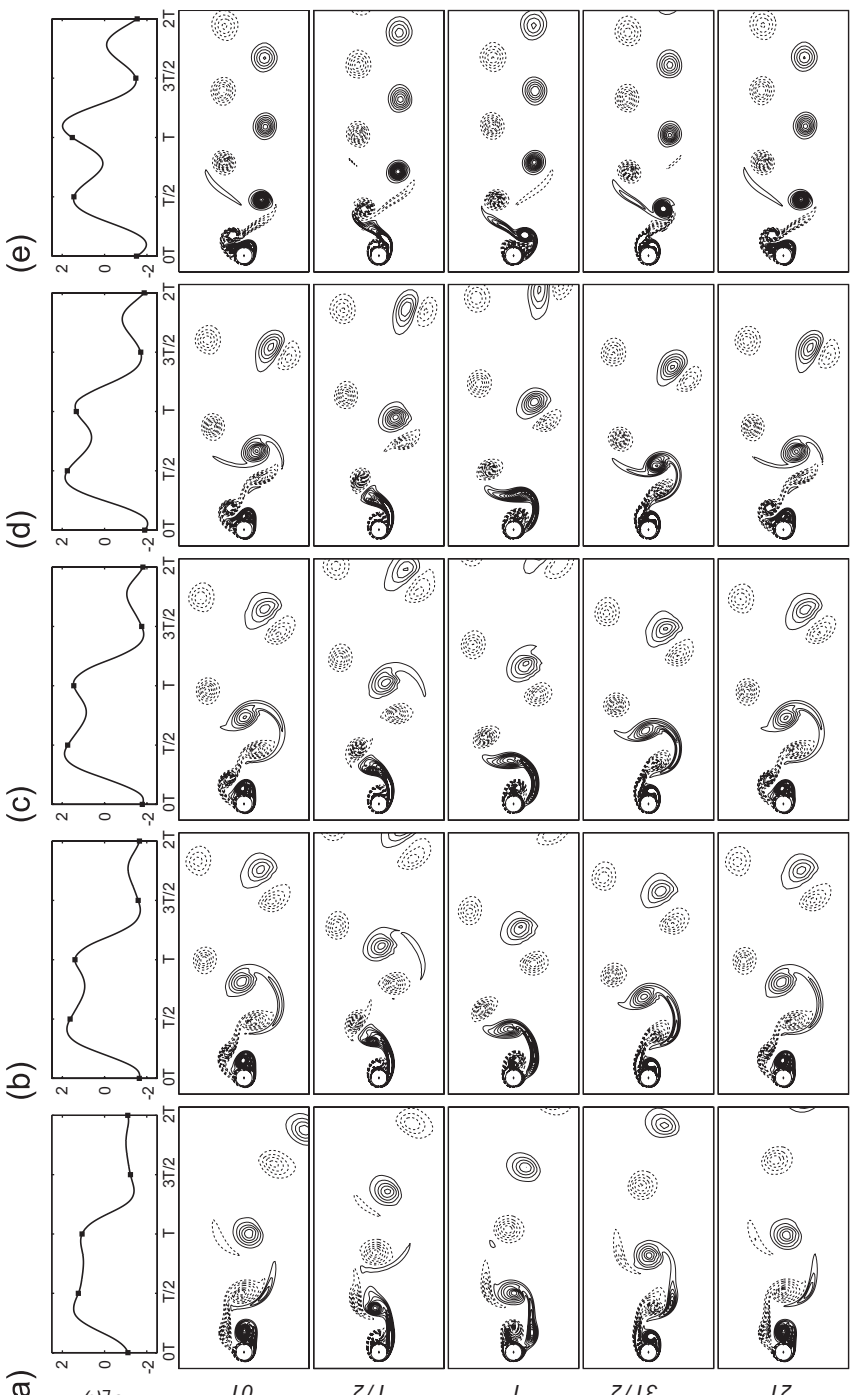

Fig. 13. Equivorticity lines over two periods of oscillation, $2T$, for $R = 200$, $A = 0.3$: (a) $f/f_0 = 1.10$; (b) $f/f_0 = 1.30$; (c) $f/f_0 = 1.40$; (d) $f/f_0 = 1.50$; (e) $f/f_0 = 1.80$. The instantaneous snapshots are marked in the corresponding lift coefficient curve shown above the snapshots for each frequency.

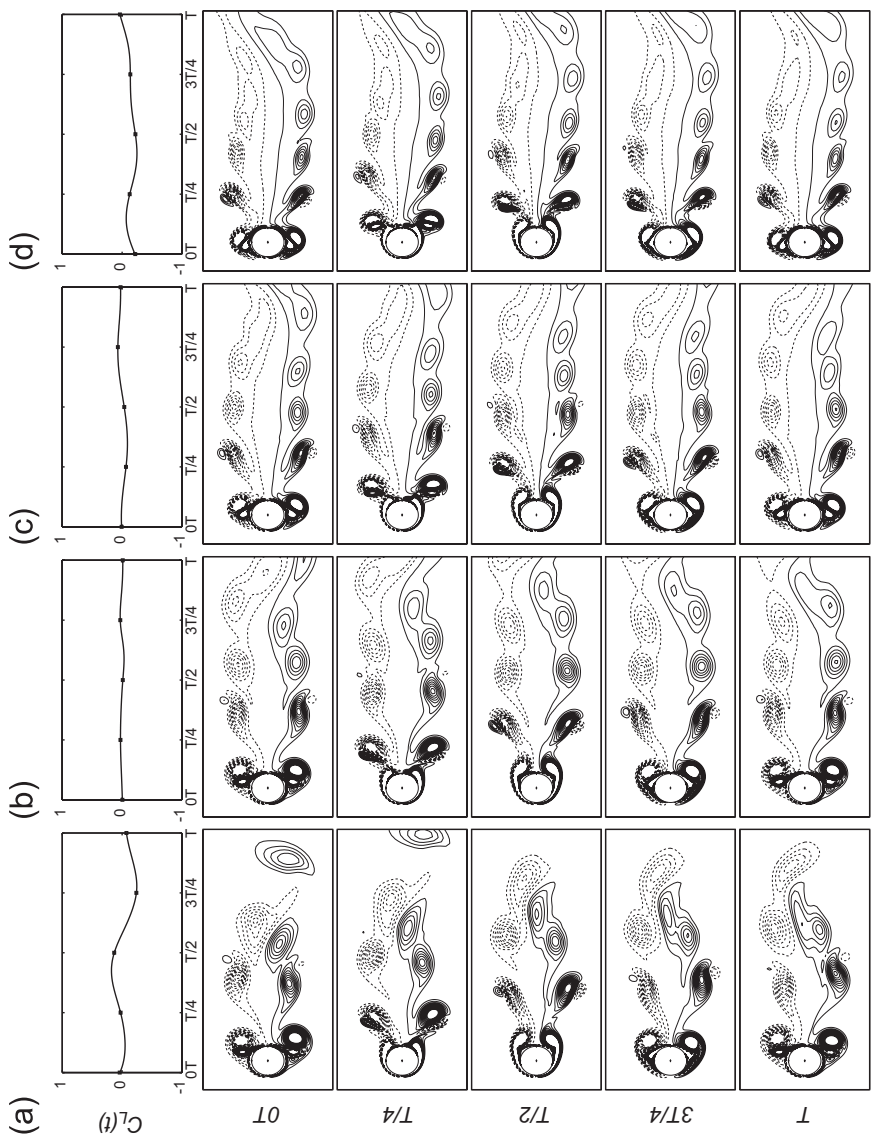

Fig. 14. Equivorticity lines over two periods of oscillation, $2T$, for $R = 200$, $A = 0.3$: (a) $f/f_0 = 1.85$; (b) $f/f_0 = 2.0$; (c) $f/f_0 = 2.5$; (d) $f/f_0 = 3.0$. The instantaneous snapshots are marked in the corresponding lift coefficient curve shown above the snapshots for each frequency.

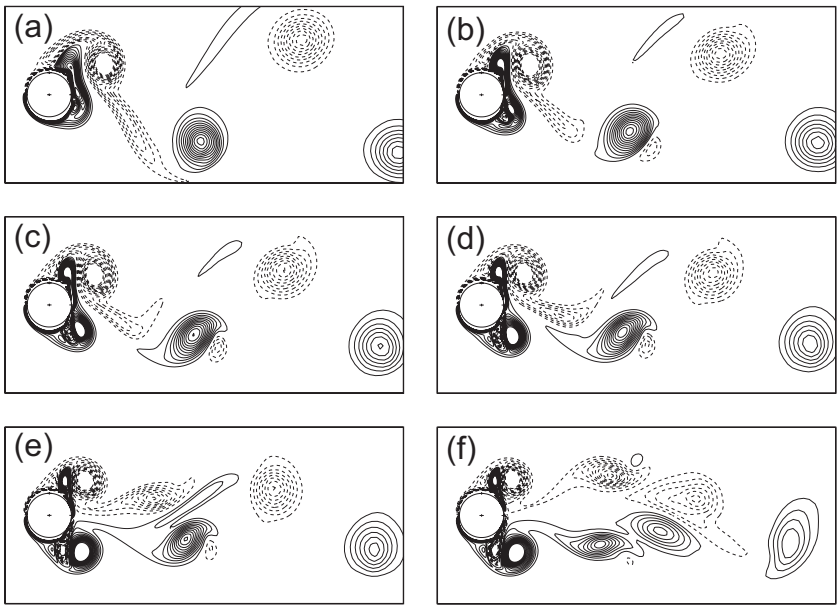

Fig. 15. Equivorticity lines at an instant corresponding to the maximum positive displacement for $R = 200$, $A = 0.3$: (a) $f/f_0 = 1.80$; (b) $f/f_0 = 1.81$; (c) $f/f_0 = 1.82$; (d) $f/f_0 = 1.83$; (e) $f/f_0 = 1.84$; (f) $f/f_0 = 1.85$.

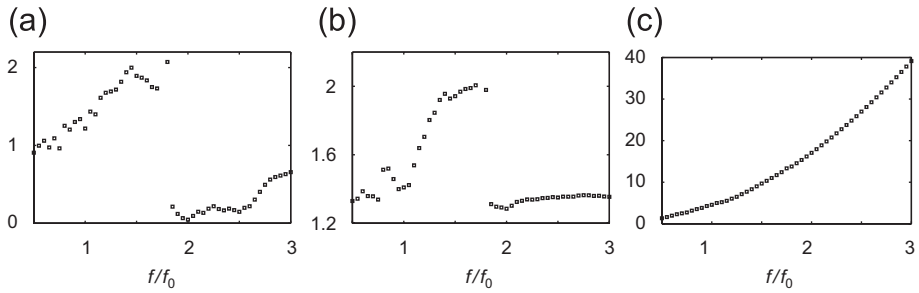

Fig. 16. Effect of f/f_0 on (a) $C_{L,\max}$; (b) $\bar{C}_D$; (c) $C_{D,\text{amp}}$, when $R = 200$, $A = 0.3$.

Further insight into the transition from the asymmetrical to symmetrical modes of vortex-shedding is shown in Fig. 15. Equivorticity contours for $f/f_0 = 1.80, 1.81, 1.82, 1.83, 1.84, 1.85$ are displayed at the instant corresponding to the maximum positive displacement of cylinder. A reduction in the upper vortex-shedding layer and an increase in the strength of the bottom shedding vortex is captured as f/f_0 increases. This mechanism continues until the strength of the upper and lower vortices becomes the same, resulting in the symmetric vortex pair mode.

Fig. 16 displays results from the fluid forces acting on the surface of the cylinder as a function of the frequency ratio f/f_0. Figs. 16(a), (b) and (c), respectively, show $C_{L,\max}$, $\bar{C}_D$ and $C_{D,\text{amp}}$. The jump and significant reduction in $\bar{C}_D$ and $C_{L,\max}$ at $f/f_0 = 1.85$ is observed as the wake makes a transition from its asymmetric form to the symmetric form. This transition, however, has no effect on the amplitude of the drag coefficient, $C_{D,\text{amp}}$, which steadily increases as f/f_0 increases. An increase in the drag coefficient amplitude is also observed for increasing amplitude of oscillation (compare with $A = 0.1$, Fig. 11).

4. Concluding remarks

A comprehensive analysis of locked-on flow regimes, determined numerically, and analyzed in terms of near-wake equivorticity contours and Lissajous patterns of unsteady lift coefficient, is presented as a result of forced streamwise cylinder oscillations in a uniform stream. Two-dimensional numerical simulations are conducted at $R = 200 : A = 0.1, 0.3$ and $0.5 \leqslant f/f_0 \leqslant 3.0$ using an accurate spectral finite-difference method. The well-known lock-on range ($f/f_0 \approx 2.0$) for the

streamwise oscillations is verified at $R = 200$ and $A = 0.1, 0.3$. Lock-on ranges are larger with the increase of the amplitude from 0.1 to 0.3, reflecting the dominance of the oscillatory motion over the uniform translation for increasing amplitude. Symmetric and antisymmetric locked-on modes are observed as the amplitude of oscillation increased. Resulting modes are consistent with the modes observed in several previous free and forced oscillation studies [see, e.g., Ongoren and Rockwell (1988)]. We note that Ongoren and Rockwell conducted their experiments at a fixed oscillation amplitude of $A = 0.13$ (i.e., the effect of increasing amplitude on near-wake is not investigated). At low amplitude, lock-on transition from the 2P to 2S mode per $2T$ is observed in the range $1.5 \leqslant f/f_0 \leqslant 2.2$, corresponding to a significant increase in the fluid forces near $f/f_0 = 2.0$. Then, transition to the lock-on S+P mode per $3T$ occurs at $f/f_0 = 2.8$. The transition state is observed from six shed vortices (per $3T$) to the P+S mode per $3T$ at $f/f_0 = 2.8$. This results from the coalescence of three shed vortices from upper side of the cylinder and the coalescence of two of the three vortices developing on the bottom side of the cylinder over three periods of cylinder oscillation. This phenomenon is not observed for other values of the forcing frequency ratios. The symmetric vortex-shedding mode is observed for increasing forcing frequency at $A = 0.3$, whereas the flow is entirely asymmetric for $A = 0.1$. This is consistent with the experimental findings of Konstantinidis et al. (2005) who reported that the wake pattern does not change and remains at the asymmetric 2S mode, for relatively low amplitudes ($0.042 \leqslant A \leqslant 0.053$). The transition from asymmetric to symmetric vortex-shedding modes and its relation to the fluid forces are also discussed. Due to the symmetrical flow component, the lift force shows a dramatic decrease as the symmetric modes develop in the wake.

Acknowledgments

The financial support for this research is provided by the Natural Sciences and Engineering Research Council of Canada. Preliminary results of this research are reported at various conferences; see, e.g., Lawrence et al. (2003), Al-Mdallal et al. (2003).

References

Al-Mdallal, Q., 2004. Analysis and computation of the cross-flow past an oscillating cylinder with two degrees of freedom. Ph.D. Thesis, Memorial University of Newfoundland, St. John's, Canada.

Al-Mdallal, Q., Lawrence, K.P., Kocabiyik, S., 2003. Numerical study of streamwise oscillations of a cylinder in a steady current. Part 2: vortex formation mode competition. Bulletin of the American Physical Society, 8, Poster # 13.

Anagnostopoulos, P., 2000. Numerical study of the flow past a cylinder excited transversely to the incident stream. Part 1: lock-in zone, hydrodynamic forces and wake geometry. Journal of Fluids and Structures 14, 819–851.

Anagnostopoulos, P., 2002. Flow-Induced Vibrations in Engineering Practice. WIT Press, Ashurst, UK.

Badr, H.M., Dennis, S.C.R., 1985. Time-dependent viscous flow past an impulsively started rotating and translating circular cylinder. Journal of Fluid Mechanics 158, 447–488.

Badr, H.M., Dennis, S.C.R., Kocabiyik, S., Nguyen, P., 1995. Viscous oscillatory flow about a circular cylinder at small to moderate Strouhal number. Journal of Fluid Mechanics 303, 215–232.

Barbi, C., Favier, D., Maresca, C., Telionis, D., 1986. Vortex shedding and lock-on of a cylinder in oscillatory flow. Journal of Fluid Mechanics 170, 527–544.

Bearman, P.W., 1984. Vortex shedding from oscillating bluff bodies. Annual Review of Fluid Mechanics 16, 195–222.

Braza, M., Chassaing, P., Minh, H.H., 1986. Numerical study and physical analysis of the pressure and velocity fields in the near wake of a circular cylinder. Journal of Fluid Mechanics 165, 79–130.

Cetiner, O., Rockwell, D., 2001. Streamwise oscillations of a cylinder in a steady current. Part 1: locked-on stages of vortex formation and loading. Journal of Fluid Mechanics 427, 1–28.

Chang, K.-S., Sa, J.-Y., 1992. Patterns of vortex shedding from an oscillating circular cylinder. AIAA Journal 30, 1331–1336.

Cheng, M., Chew, Y.T., Luo, S.C., 1997. A hybrid vortex method for flows over a bluff body. International Journal for Numerical Methods in Fluids 24, 253–274.

Clift, R., Grace, J.R., Weber, M.E., 1978. Bubbles, Drops, and Particles. Academic Press, London, UK.

Collins, W.M., Dennis, S.C.R., 1973a. Flow past an impulsively started circular cylinder. Journal of Fluid Mechanics 60, 105–127.

Collins, W.M., Dennis, S.C.R., 1973b. The initial flow past an impulsively started circular cylinder. The Quarterly Journal of Mechanics and Applied Mathematics 26, 51–75.

Dennis, S.C.R., Chang, G.Z., 1969. Numerical integration of the Navier–Stokes equations, Technical Summary Report No. 859. Mathematical Research Center, University of Wisconsin, USA.

Dennis, S.C.R., Kocabiyik, S., 1991. An asymptotic matching condition for unsteady boundary-layer flows governed by the Navier–Stokes equations. IMA Journal of Applied Mathematics 47, 81–98.

Dennis, S.C.R., Quartapelle, L., 1989. Some used of Green's theorem in solving the Navier–Stokes equations. International Journal for Numerical Methods in Fluids 9, 871–890.

Graham, J.M.R., Arkell, R.H., Zhou, C.-Y., 1993. The effect of combinations of mean current and oscillatory flow on the forces induced on a bluff body. Journal of Wind Engineering and Industrial Aerodynamics 50, 85–96.

Griffin, O.M., Hall, M.S., 1991. Review-vortex shedding lock-on and flow control in bluff body wakes. ASME Journal of Fluids Engineering 113, 526–537.

Griffin, O.M., Ramberg, S.E., 1976. Vortex shedding from a cylinder vibrating in line with incident uniform flow. Journal of Fluid Mechanics 75, 257–271.

Hurlbut, S.E., Spaulding, M.L., White, F.M., 1982. Numerical solution for laminar two dimensional flow about a cylinder oscillating in a uniform stream. ASME Journal of Fluids Engineering 104, 214–221.

Jauvtis, N., Williamson, C., 2004. The effect of two degrees of freedom on vortex-induced vibration at low mass and damping. Journal of Fluid Mechanics 509, 23–62.

Justesen, P., 1991. A numerical study of oscillating flow around a circular cylinder. Journal of Fluid Mechanics 222, 157–196.

Karanth, D., Rankin, G.W., Sridhar, K., 1995. Computational study of flow past a cylinder with combined in-line and transverse oscillation. Computational Mechanics 16, 1–10.

Kim, B.-H., 2000. Quadratic nonlinear behavior of surface pressures on cylinders undergoing forced oscillations. Master's Thesis, Illinois Institute of Technology, Chicago, USA.

King, R., 1974. Vortex excited structural oscillations of a circular cylinder in steady currents. OTC Paper 1948. Sixth Annual Offshore Technology Conference. Houston, TX, USA.

King, R., 1977. A review of vortex shedding research and its application. Ocean Engineering 4, 141–172.

King, R., Prosser, M., Johns, D.J., 1973. On vortex excitation of model piles in water. Journal of Sound and Vibration 29, 169–188.

Kocabiyik, S., Mahfouz, F.M., Al-Mdallal, Q., 2004. Numerical simulation of the flow behind a circular cylinder subject to small-amplitude recti-linear oscillations. Advances in Engineering Software 35, 619–631.

Konstantinidis, E., Balabani, S., Yianneskis, M., 2005. The timing of vortex shedding in a cylinder wake imposed by periodic inflow perturbations. Journal of Fluid Mechanics 543, 45–55.

Koumoutsakos, P., Leonard, A., 1995. High-resolution simulations of the flow around an impulsively started cylinder using vortex methods. Journal of Fluid Mechanics 296, 1–38.

Lawrence, K.P., 2004. Computation of unsteady viscous incompressible flow around an obliquely oscillating circular cylinder using a parallelized finite difference algorithm. Master's Thesis, Memorial University of Newfoundland, Newfoundland, Canada.

Lawrence, K.P., Al-Mdallal, Q., Kocabiyik, S., 2003. Numerical study of streamwise oscillations of a cylinder in a steady current. Part 1: locked-on states of vortex formation. Bulletin of the American Physical Society, 8, Poster # 13.

Lecointe, Y., Piguet, J., 1989. Flow structure in the wake of an oscillating cylinder. ASME Journal of Fluids Engineering 111, 139–148.

Martinez, G., Hinh, H.H., 1978. In: Proceedings of International Conference on Numerical Methods in Laminar and Turbulent Flow, Pineridge, Swansea, pp. 105–127.

Matsumoto, M., 1999. Vortex shedding of bluff bodies: a review. Journal of Fluids and Structures 13, 791–811.

Mittal, S., Ratner, A., Hastreiter, D., Tezduyar, T., 1991. Space–time finite element computation of incompressible flows with emphasis on flows involving oscillating cylinders. International Video Journal of Engineering Research 1, 83–96.

Nakamura, A., Okajima, A., Kosugi, T., 2001a. Experiments and flow-induced in-line oscillation of a circular cylinder in a water tunnel 1st report: the difference of the response characteristics when a cylinder is elastically supported at both end and cantilevered. JSME International Journal, Fluids and Thermal Engineering, Series B, 695–704.

Nakamura, A., Okajima, A., Kosugi, T., 2001b. Experiments and flow-induced in-line oscillation of a circular cylinder in a water tunnel. 2nd report: influence of the aspect ratio of a cantilevered circular cylinder. JSME International Journal, Fluids and Thermal Engineering, Series B, 705–711.

Naudascher, E., 1987. Flow-induced streamwise vibrations of structures. Journal of Fluids and Structures 1, 257–271.

Naudascher, E., Rockwell, D., 1994. Flow-Induced Vibrations: An Engineering Guide. A.A. Balkema, Rotterdam, Netherlands.

Nishihara, T., Kaneko, S., Watanbe, T., 2005. Characteristics of fluid dynamic forces acting on a circular cylinder oscillated in the streamwise direction and its wake patterns. Journal of Fluids and Structures 20, 505–518.

Okajima, A., Kosugi, T., Nakamura, A., 2002. Flow-induced in-line oscillation of a circular cylinder in a water tunnel. ASME Journal of Pressure Vessel Technology 124, 89–96.

Okajima, A., Nakamura, A., Kosugi, T., Uchida, H., Tamaki, R., 2004. Flow-induced in-line oscillation of a circular cylinder. European Journal of Mechanics B/Fluids 23, 115–125.

Ongoren, A., Rockwell, D., 1988. Flow structure from an oscillating cylinder. Part 2: mode competition in the near wake. Journal of Fluid Mechanics 191, 225–245.

Pier, B., Huerre, P., 2001. Nonlinear self-sustained structures and fronts in spatially developing wake flows. Journal of Fluid Mechanics 435, 145–174.

Qian, L., Vezza, M., 2001. A vorticity-based method for incompressible unsteady flows. Journal of Computational Physics 172, 515–542.

Sakai, T., Iwata, K., Morishita, M., Kitamura, S., 2001. Vortex-induced vibration of a cantilever circular cylinder in super-critical Reynolds number flow and its suppression by structure damping. JSME International Journal, Fluids and Thermal Engineering, Series B 44, 712–720.

Sarpkaya, T., 1979. Vortex induced oscillations. Journal of Applied Mechanics 46, 241–258.

Sarpkaya, T., 2004. A critical review of the intrinsic nature of vortex induced vibrations. Journal of Fluids and Structures 19, 389–447.
Sarpkaya, T., Putzig, C., Gordon, D., Wang, X., Dalton, C., 1992. Vortex trajectories around a circular cylinder in oscillatory plus mean flow. ASME Journal of Offshore Mechanics and Arctic Engineering 114, 291–298.
Schlichting, H., 2000. Boundary Layer Theory, eighth ed. Springer, New York.
Sumer, B.M., Fredsøe, J., 1997. Hydrodynamics Around Cylindrical Structures. World Scientific, Singapore.
Tanida, Y., Watanabe, A.O.Y., 1973. Stability of a circular cylinder oscillating in a uniform flow or in a wake. Journal of Fluid Mechanics 61, 769–784.
VanDyke, M., 1982. An Album of Fluid Motion. The Parabolic Press, Stanford.
Williamson, C.H.K., Govardhan, R., 2004. Vortex-induced vibrations. Annual Review of Fluid Mechanics 36, 413–455.
Williamson, C.H.K., Roshko, A., 1988. Vortex formation in the wake of an oscillating cylinder. Journal of Fluids and Structures 2, 355–381.
Wootton, L., Warner, M., Cooper, D., 1974. Some aspects of the oscillations of full-scale piles. In: Naudascher, E. (Ed.), Flow-Induced Structural Vibrations. Springer-Verlag, Berlin, pp. 587–601.
Zdravkovich, M.M., 1996. Different modes of vortex shedding: an overview. Journal of Fluids and Structures 10, 427–437.
Zdravkovich, M.M., 1997. Flow Around Circular Cylinders: vol. 1: Fundamentals. Oxford University Press, Oxford.